Project Report on
"Experimental Study of Thermal Pressurization and the Role of Fault Roughness"

INTRODUCTION

We have been studying the widely discussed dynamic weakening mechanism termed *thermal pore-fluid pressurization*. There are many theoretical and numerical studies of thermal pressurization [*Andrews*, 2002; *Lachenbruch*, 1980; *Lee and Delaney*, 1987; *Mase and Smith*, 1985; 1987; *Noda*, 2008; *Noda and Shimamoto*, 2005; *Rempel and Rice*, 2006; *Rice*, 2006; *Rice and Cocco*, 2007; *Sibson*, 1973] and it is increasingly used in dynamic rupture and earthquake nucleation models [*Bizzarri and Cocco*, 2006a; b; *Lapusta and Rice*, 2004a; b; *Noda et al.*, 2009; *Noda and Lapusta*, 2010; *Rice et al.*, 2010; *Schmitt and Segall*, 2009; *Segall and Rice*, 2006]. Although more study is needed, our experiment studies of thermal pressurization are the most definitive ones yet obtained.

With SCEC 2018 funding we continued experiments funded in previous years to further investigate fault-weakening via thermal pore-fluid pressurization. This report presents new results obtained in the last year. One of our goals has been to understand the role that fault-roughness-induced dilatancy may play in defeating this weakening mechanism on natural faults. In a previous grant period we conducted one complicated experiment with an initially mated fault surface with high roughness and considerable dilatancy that, as expected, showed no weakening. However, in some other experiments where thermal pressurization weakening was expected it did not occur. Before continuing to investigate the role of roughness we need to ensure reproducibility, i.e. that weakening always occurs when conditions predict that it should. The fact that this has not always been the case suggested that there was some uncontrolled variable that we could not identify. During the past few months we believe we have discovered the problem. We have found that for some samples the fluid in the fault zone has been able to escape via a high permeability path along the margins of the samples. The epoxy that secures the samples to the steel sample grips also is supposed to create a fluid-tight seal. In some cases this was not the case, as we showed (after the experiment) by being able to blow air along this epoxied boundary. The data supporting this are not included in this report for space reasons. We did no experiments using rough initially mated surfaces this year since we first needed to identify our uncontrolled variable. Rather, we show the contrast between dry samples and those that are fluid saturated with a known uniform initial pore fluid pressure of water for samples with different permeabilities. We also report on possible explanations for some difference between our observed weakening and theoretical predictions.

RESULTS

In the following section we present results from permeability measurements and velocity step experiments. First, we report the pressure-dependent permeability of Frederick diabase for select samples (Figure 1). The tendency for pore fluids to become pressurized during shear heating is directly dependent on the permeability of the host rock. Next, we show results on the evolution of friction during velocity step experiments at: (1) Dry conditions (Figure 2), and (2) Undrained water-saturated conditions with known initial pore pressure (Figure 3). With dry conditions in the fault zone, friction increases with velocity – indicating velocity-strengthening behavior at the tested conditions. However, under undrained wet conditions, significant dynamic weakening occurs, indicating thermo-hydraulic coupling, even at sub-seismic slip rates of millimeters per second. All experiments were conducted with an effective normal stress $\sigma = 25\ MPa$, effective confining pressure $P = 20\ MPa$, and pore pressure of $P_p = 25\ MPa$, unless stated otherwise. Finally, we present results of an analysis of the stress state in our samples that suggests tensile cracks may form and could act as a reservoir and increase hydraulic diffusivity, both of which would reduce the fluid pressure.

Permeability of Frederick diabase

Plots of permeability versus effective confining pressure are illustrated for selected samples in Figure 1. The permeability was estimated using a Darcy flow-through experiment for sample 346 and a pore

pressure oscillation experiment [e.g., *Fischer*, 1992] for sample 340. Sample 340 underwent heat treatment at 630°C, while sample 346 was heat treated to 530°C. Accordingly, the permeability of sample 346 was ~1 order of magnitude lower than the other sample.

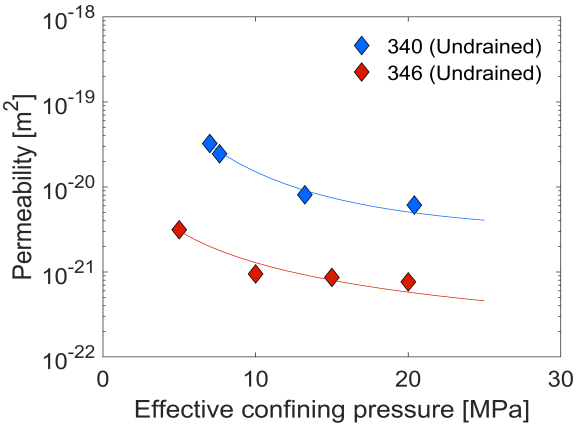

Figure 1. Permeability results for two undrained samples.

Dry friction

The dry (at room humidity of 35%) frictional response is illustrated in Figure 2 for velocity step-ups from a reference velocity $v_0 = 3.162\ \mu m/s$ to $v = 2.5\ mm/s$ (a) and $v = 5\ mm/s$ (b) and then back down to the reference velocity. These data show velocity-strengthening behavior, with an increase in friction at the step-up, after which friction remains elevated, without an obvious evolution to steady-state. The frictional behavior can be fit by a logarithmic law following the "direct effect" in rate-and -state friction:

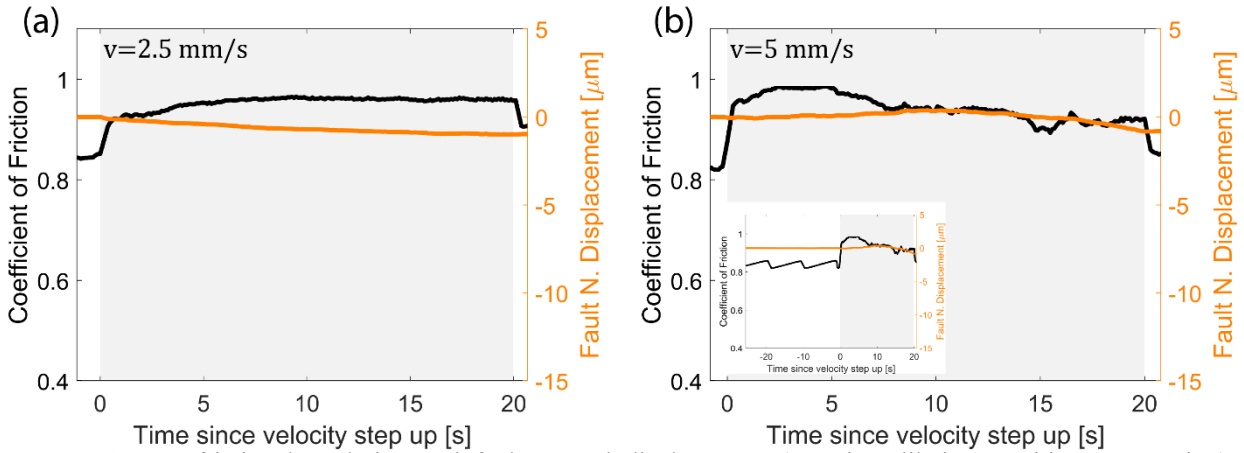

Figure 2. Dry frictional evolution and fault normal displacement (negative=dilation, positive=compaction) during a velocity step, from base velocity $v_0 = 3.162\ \mu m/s$ (unshaded areas) to high velocity v (shaded areas); (A) $v = 2.5\ mm/s$, (B) $v = 5\ mm/s$. Note the slow stick-slip events before the velocity step in the inset in B. Fault-normal displacement is $< 1\ \mu m$ during a velocity step with little change in either the step up ($v_0 \rightarrow v$) or the step down ($v \rightarrow v_0$).

$$\mu = \mu_0 + a\log(V/V_0)\,, \qquad (1)$$

where μ is the coefficient of friction, V is the sliding velocity and a is a scaling factor. The subscript 0 denotes the parameter at the initial steady-state (here, during sliding at the reference velocity). The factor a is estimated here to be in the range 0.011-0.017. In accordance with (4), after the velocity is stepped back down to the reference velocity, friction decreases.

Wet friction under undrained conditions

The evolution of friction with undrained conditions is illustrated for two different samples in Figure 3 for velocity steps from v_0 to $v = 2.5\ mm/s$, then back to v_0. The total displacement accumulated on these samples before the velocity steps was relatively small; 10 mm and 26 mm for samples 340 (Figure 3a) and 346 (Figure 3b), respectively. These data differ significantly from the dry (Figure 2) case. At the velocity step-up, friction increases as in the previous cases, but this increase is followed by dramatic weakening during which the friction drops by 43% and 52% (Figure 3a and Figure 3b, respectively).

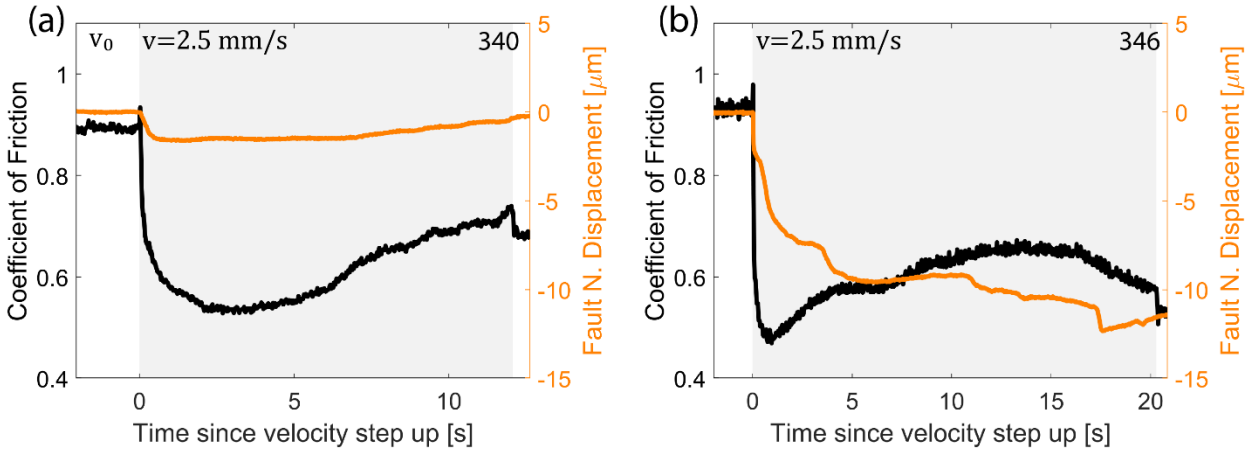

Figure 3. Friction and fault normal displacement during a velocity step from base velocity $v_0 = 3.162\ \mu m/s$ to $v = 2.5\ mm/s$, for samples 340 (a) and 346 (b). A transient increase in friction is observed during the step up, followed by dramatic weakening. Afterward the fault regains some of its original strength. Note the big difference in the amount of dilation between these samples, with about 10 times more dilation in sample 346 (a) than sample 340 (b).

However, this weakening is not maintained throughout the entire course of the high velocity interval, namely friction increases after the initial stage of weakening. For sample 340 (Figure 3a), the increase is gradual. Sample 346 (Figure 3b) exhibits a faster transition from weakening to strengthening, and it weakens again in the final stages of the velocity step. Note however that both samples underwent strengthening to high-speed displacements of 30 mm (12 seconds). Whether the final weakening in sample 346 would have occurred for sample 340 if more high-speed displacement were imposed on sample 340 is unknown. The most notable difference between the two samples is the shorter displacement over which the initial high-speed weakening occurred in the less permeable sample 346.

The fault normal displacements during the high speed sliding differ from one another and from those observed during the dry experiments (Figure 2). Both undrained samples dilate significantly after the velocity increase, unlike the dry samples. Then the more permeable sample 340 (Figure 3a) stops dilating after the initial weakening stage and the fault normal displacement remains relatively constant at around 1.5 μm, and then compacts slightly in the final stages of the high velocity interval, coincident with the observed strengthening. In contrast the less permeable sample 346 (Figure 3b) continues to dilate in pulses for the entire duration of the high velocity interval, up to a total dilation of 12 μm. Both samples exhibit a small compaction once the velocity is stepped down to base value, but this behavior is not significantly different from the dry samples.

DISCUSSION

Although weakening attributable to thermal pressurization occurs in the water-saturated low permeability samples as we have shown in the past, the subsequent transition from dynamic weakening to strengthening (Figure 3) suggest that elevated fluid pressures are not sustained in the fault zone during rapid slip. Three factors may complicate the nominally undrained conditions present in the fault zone: (1) fault dilation; (2) changes in fault drainage due to cracking; and (3) intrinsic changes in the fault zone properties.

It is unclear whether the nominally flat geometry of the tested faults in this study would invoke enough dilation to restrict thermal pressurization. The faults instantaneously dilate by 1-5 μm during the first millimeter of slip after the velocity step, which corresponds to an extremely small fluid volume of < 4.0 mm^3 right at the fault surface. How large a pressure change this volume change would correspond to

depends on the communicating volume occupied by fluid near the fault surface, which is unknown. In any case the pressure change with such a small volume change is highly susceptible to any local changes in the fault zone structure and the drainage system. Note that this dilation occurs under constant applied normal stress imposed on the fault, using our internal force gage as the servo feedback source.

Analysis of the stress orientations and magnitudes in our experiments during slip indicate that the minimum principal stress becomes tensile during a test as pore fluid pressure increases due to thermal pressurization (Figure 4), and thus microcracking near the fault surface might occur. The minimum principal stress (σ_3) is calculated to be:

$$\sigma_3 = \frac{\sigma_n + P_c}{2} - p - \sqrt{\left[\frac{\sigma_n - P_c}{2}\right]^2 + [\mu(\sigma_n - p)]^2} \quad (2)$$

where σ_n is the normal stress, P_c is the confining pressure, p is the pore fluid pressure and μ is the coefficient of friction. Figure 4 shows that at the initial experimental conditions ($\frac{p}{P_c}$~0.56, $\mu = 0.9$) the minimum principal stress is close to zero. As pore pressure increases the minimum principal stress becomes more tensile (Figure 4), which would accommodate opening of microcracks in the vicinity of the fault. Such microcracks can both serve as a reservoir and increase the fluid diffusivity, as discussed next.

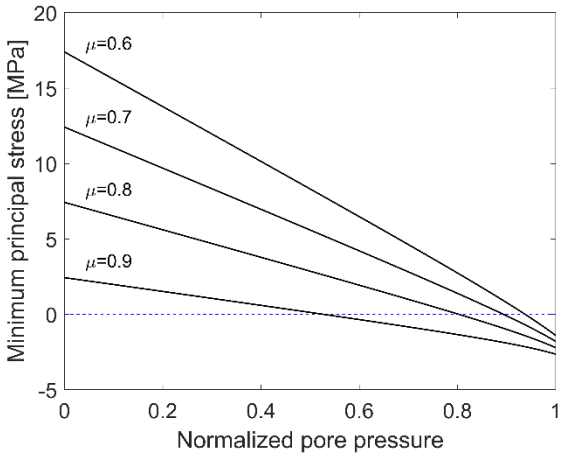

Figure 1. Minimum principal stress as a function of pore pressure during a thermal pressurization experiment, for different coefficients of friction μ. Pore pressure p is normalized by the confining pressure P_c, the dashed blue line represents zero stress – above it stresses are compressive, below it stresses are tensile.

The compressibility will be higher in the presence of microcracks. The change in compressibility is expected [*Brantut and Mitchell,* 2018] to affect both the pressurization factor (Λ) and the storage capacity (S), as defined by *Rice* [2006]:

$$\Lambda = \frac{\lambda_f - \lambda_n}{\beta_f + \beta_n}, \quad (3)$$

$$S = n(\beta_f + \beta_n), \quad (4)$$

where λ_f and λ_n are the thermal expansivities of the fluid and pores, respectively, β_f is the compressibility of the fluid and n is the porosity. *Brantut and Mitchell* [2018] point out that an increase in β_n would have two competing effects: Λ would decrease and S would increase. The change in S would prompt a decrease in the hydraulic diffusivity

$$\alpha_{hy} = k/\eta S \quad (5)$$

where η is the fluid viscosity and k is the permeability. The decrease in hydraulic diffusivity would favor thermal pressurization, opposed to a decrease in the pressurization factor Λ which slows thermal pressurization. Their analysis suggests that the latter effect is the more dominant and thus the overall behavior supports slower pressurization rates in more hydraulically compliant fault zones. Moreover, β_n, n and k are all functions of fluid pressure, which makes the expected behavior during thermal pressurization more complex and difficult to predict. *Rice's* [2006] solution is given for constant

hydraulic parameters and does not consider changes in α_{hy} and Λ. In order to resolve this uncertainty, it is necessary to generalize the model to include the effect of changes of fluid pressure on Λ and α_{hy} during thermal pressurization. Taking into account the fluid pressure dependence of permeability (Figure 4):

$$k = k_0 + a(P_c - p)^b \,, \tag{6}$$

porosity [*K. Okazaki, personal communication*]:

$$n = c(P_c - p)^d \,, \tag{7}$$

and the relation between pore compressibility (β_n) and porosity [*Rice,* 2006]:

$$\beta_n = \frac{(\beta_d - \beta_s)(\beta_d + r\beta_s)}{n(1+r)\beta_d} - \beta_s \,, \tag{8}$$

where k_0, a, b, c, d are constants, P_c is the confining pressure, p is the pore pressure, β_d is the drained compressibility of the rock, β_s is the compressibility of the solid skeleton and r is a function of the drained Poisson's ratio of the rock. Figure 5 presents the results of this analysis; as pore pressure increases both the pressurization factor Λ and the hydraulic diffusivity α_{hy} increase. However, Λ increases by less than a factor of 1.5 while α_{hy} increases by a factor of ~ 11. While this simplistic approach assumes constant η, β_d, β_s and r, it demonstrates that the rheology of a fault during thermal pressurization can be affected by fluid-pressure-induced changes in the properties of the adjacent elastic layer.

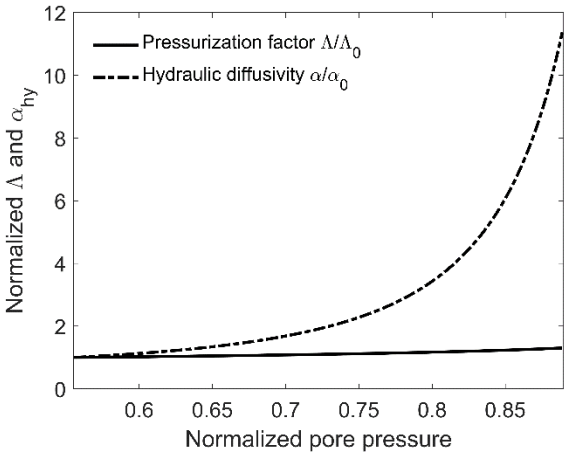

Figure 2. Variations of pressurization factor Λ and hydraulic diffusivity α_{hy} with pore fluid pressure. Λ and α_{hy} are normalized by their initial value, pore pressure is normalized by the confining pressure.

In summary, the creation of microcracks during thermal pressurization could both create a local reservoir for fluid and could increase the fluid diffusivity. Both of these could be responsible for reducing any increase in pore pressure from what it would have been without the new microcracks and might explain why the shear strength increases during the fast sliding following the initial large decrease (Figure 3).

In last year's report we showed results of rapid sliding for experimental faults with much larger total displacements than those in Figure 3. Although those faults showed dynamic weakening, the weakening rate and magnitude is much lower than that illustrated in Figure 3. We believe this is due to the presence of a wider fault zone with more wear material due to the larger total displacement. This wear material material would be expected to have a higher compressibility than the intact rock and therefore a higher hydraulic diffusivity as shown in Figure 5. This could explain the lower rate and magnitude of dynamic weakening for the large total-displacement faults.

Our experimental results suggest that existing theoretical treatments of thermal pressurization [e.g. *Rice,* 2006] may neglect some important factors that can alter the results from those expected. In particular our results suggest that the expected increase in fluid pressure during thermal pressurization will increase the pore fluid diffusivity and, at least for our experimental geometry, may cause structural damage due to development of tensile stresses in the fault. Our calculations show that these structural and hydraulic changes may be responsible for inhibiting further weakening and may even reduce the fluid pressure and thereby promote frictional strengthening as observed in our experimental faults.

References Cited

Andrews, D. J. (2002), A fault constitutive relation accounting for thermal pressurization of pore fluid, *J. Geophys. Res.*, *107*, 12.

Bizzarri, A., and M. Cocco (2006a), A thermal pressurization model for the spontaneous dynamic rupture propagation on a three-dimensional fault: 1. Methodological approach, *J. Geophys. Res.*, *111*, B05303, doi:05310.01029/02005JB003862.

Bizzarri, A., and M. Cocco (2006b), A thermal pressurization model for the spontaneous dynamic rupture propagation on a three-dimensional fault: 2. Traction evolution and dynamic parameters, *J. Geophys. Res.*, *111*, B05304, doi:05310.01029/02005JB003864.

Brantut, N., & Mitchell, T. M. (2018). Assessing the efficiency of thermal pressurization using natural pseudotachylyte - bearing rocks. *Geophysical Research Letters, 45*(18), 9533-9541.

Fischer, G. J. (1992), The determination of permeability and storage capacity: pore pressure oscillation method, in *Fault mechanics and transport properties of rocks*, edited by B. Evans and T.-f. Wong, pp. 187-211, Academic Press, New York.

Lachenbruch, A. H. (1980), Frictional heating, fluid pressure, and the resistance to fault motion, *J. Geophys. Res.*, *85*, 6249-6272.

Lapusta, N., and J. R. Rice (2004a), Earthquake sequences on rate and state faults with strong dynamic weakening, paper presented at 2004 SCEC Annual Meeting Proceedings and Abstracts, Southern California Earthquake Center, PalmSprings, California, 2004.

Lapusta, N., and J. R. Rice (2004b), Earthquake sequences on rate and state faults with strong dynamic weakening, *Eos. Trans. Am. Geophys. Union, Fall Meeting Suppl.*, *85*(47), T22A-05.

Lee, T. C., and P. T. Delaney (1987), Frictional Heating and Pore Pressure Rise Due to a Fault Slip, *Geophysical Journal of the Royal Astronomical Society*, *88*(3), 569-591.

Mase, C. W., and L. Smith (1985), Pore-fluid pressures and frictional heating on a fault surface, *Pure Appl. Geophys.*, *122*, 583-607.

Mase, C. W., and L. Smith (1987), Effects of frictional heating on the thermal hydrologic and mechanical response of a fault, *J. Geophys. Res.*, *92*, 6249-6272.

Noda, H. (2008), Frictional constitutive law at intermediate slip rates accounting for flash heating and thermally activated slip process, *J. Geophys. Res.*, doi:10.1029/2007JB005406.

Noda, H., E. M. Dunham, and J. R. Rice (2009), Earthquake ruptures with thermal weakening and the operation of major faults at low overall stress levels, *J. Geophys. Res.*, *114 (B07302)*, doi:10.1029/2008JB006143.

Noda, H., and N. Lapusta (2010), Three-dimensional earthquake sequence simulations with evolving temperature and pore pressure due to shear heating: Effect of heterogeneous hydraulic diffusivity, *J. Geophys. Res.*, *115*, B12314.

Noda, H., and T. Shimamoto (2005), Thermal pressurization and slip-weakening distance of a fault: An example of the Hanaore fault, southwest Japan, *Bull. Seis. Soc. Am.*, *95*(4), 1224-1233.

Rempel, A. W., and J. R. Rice (2006), Thermal pressurization and onset of melting in fault zones, *Journal of Geophysical Research-Solid Earth*, *111*(B9), B09314, doi:09310.01029/02006JB004314.

Rice, J. R. (2006), Heating and weakening of faults during earthquake slip, *Journal of Geophysical Research-Solid Earth*, *111*(B5), doi:10.1029/2005JB004006.

Rice, J. R., and M. Cocco (2007), Seismic fault rheology and earthquake dynamics, in *The Dynamics of Fault Zones*, edited by M. R. Handy, p. in press, MIT Press, Cambridge, Mass.

Rice, J. R., E. M. Dunham, and H. Noda (2010), Thermo- and hydro-mechanical processes along faults during rapid slip, in *Meso-Scale Shear Physics in Earthquake and Landslide Mechanics*, edited by Y. Hatzor, J. Sulem and I. Vardoulakis, pp. 3-16, CRC Press.

Schmitt, S. V., and P. Segall (2009), Thermal pressurization during “slip law” frictional earthquake nucleation, *Poster, 2009 SCEC Annual Meeting*.

Segall, P., and J. R. Rice (2006), Does shear heating of pore fluid contribute to earthquake nucleation?, *Journal of Geophysical Research-Solid Earth*, *111 (B09316)*, doi:10.1029/2005JB004129.

Sibson, R. H. (1973), Interactions between temperature and fluid pressure during earthquake faulting - A mechanism for partial or total stress relief, *Nature*, *243*, 66-68.